α7-Type Acetylcholine Receptor Localization and its Modulation by Nicotine and Cholesterol in Vascular Endothelial Cells

Victoria B. Ayala Peña,[1] Ida C. Bonini,[1] Silvia S. Antollini,[1] Toshihide Kobayashi,[2] and Francisco J. Barrantes[1*]

[1] *Instituto de Investigaciones Bioquímicas and UNESCO Chair of Biophysics & Molecular Neurobiology, 8000 Bahía Blanca, Argentina*

[2] *Lipid Biology Laboratory, RIKEN, 2-1, Hirosawa, Wako, Saitama 351-0198, Japan*

ABSTRACT

The neuronal-type α7 nicotinic acetylcholine receptor (α7AChR) is also found in various non-neural tissues, including vascular endothelium, where its peculiar ionotropic properties (high Ca^{2+} permeability) and its supervening Ca^{2+}-mediated intracellular cascades may play important roles in physiology (angiogenesis) and pathology (inflammation and atherogenesis). Changes in molecular (up-regulation, affinity, and conformational states) and cellular (distribution, association with membranes) properties of the α7AChR related to angiogenesis (wound-repair cell migration) and atherogenesis (alterations in cholesterol content) were studied in living endothelial cells, with the aim of determining whether such changes constitute early markers of inflammatory response. The combination of pharmacological, biochemical, and fluorescence microscopy tools showed that α7AChRs in rat arterial endothelial (RAEC) and human venous endothelial (HUVEC) cells occur at extremely low expression levels ($\sim$50 fmol/mg protein) but undergo agonist-induced up-regulation at relatively high nicotine concentrations ($\sim$300-fold with 50 μM ligand), increasing their cell-surface exposure. When analyzed in terms of cold Triton X-100 solubility and subcellular distribution, α7AChRs occur in the "non-raft" subcellular membrane fractions. Acute cholesterol depletion reduced not only cholesterol levels but also the number of cell-surface α7AChRs. Nicotine exposure markedly stimulated cell migration and accelerated wound repair, which drastically diminished in cells deprived of the sterol. The angiogenic effect of nicotine appears to be synergistic with cholesterol content. Finally, the apparent K_D of α7AChRs for the open-channel blocker crystal violet was found to be $\sim$600-fold lower in receptor-enriched membranes obtained from up-regulated HUVEC. J. Cell. Biochem. 112: 3276–3288, 2011. © 2011 Wiley Periodicals, Inc.

KEY WORDS: AORTIC AND VENOUS ENDOTHELIAL CELLS; NICOTINIC RECEPTORS; CHOLESTEROL; NICOTINE; UP-REGULATION

MATERIALS AND METHODS

CHEMICALS

Methyl-β-cyclodextrin (CDx) and crystal Violet (CrV) were purchased from Sigma Chem. Co. (St. Louis, MO). Alexa Fluor-labeled αBTX, Alexa Fluor-labeled antibodies and Laurdan were obtained from Molecular Probes (Eugene, OR). Polyclonal rabbit anti-human α7AChR (H-302) antibody was purchased from Santa Cruz Biotechnology Inc. (Santa Cruz, CA) and goat anti-rabbit antibody conjugated to horseradish peroxidase from Transduction Laboratories (Lexington, NY). Solvents were spectroscopic grade, deoxygenated by extensive nitrogen bubbling before use. The ester of polyethylene glycol-derivatized cholesterol (fPEG-Chol) was synthesized in the laboratory of Prof. T. Kobayashi as reported by Sato et al. [2004]. Anti-CD34 antibody was provided by Dr. A. Curino from this Institute.

ISOLATION AND CULTURE OF VASCULAR ENDOTHELIAL CELLS

Wistar rats (1 month old) were fed with standard rat food, given water ad libitum and maintained on a 12 h light/12 h dark cycle. Animals were sacrificed by stunning (cervical dislocation). All procedures were carried out in conformity with the Guide for the Care and Use of Laboratory Animals published by the US National Institutes of Health (NIH Publication No. 85-23, revised 1996). The thoracic aorta and endothelial cells were obtained following Yeh et al. [2002] and Cutini et al. [2009]. The thoracic aorta was dissected under aseptic conditions, removed and placed in a cold PBS solution, cleaned of adherent connective tissue, and cut into 1–1.5 mm ring segments. Special care was taken to preserve the integrity of the endothelial layer. Ring explants were seeded in Petri-dishes with Dulbecco's modified Eagle's medium (Sigma-Aldrich) supplemented with 10% fetal bovine serum, 3.7 mg sodium bicarbonate, 100 U/mL penicillin, 1 µg/mL streptomycin, 2 mM glutamine, and 2.5 µg/mL amphotericin B. Explants were cultured at 37°C in 95% air/5% CO_2 atmosphere for 4–5 days, removed from the dishes, and the remaining cells allowed to reach confluence. Cell culture purity was assessed by staining for positive immunocytochemical reactivity to endothelial cell-specific CD34 antibody and by visual inspection of their typical morphology. RAECs (rat aortic endothelial cells) were grown on 25 mm diameter polylysin-coated glass coverslips in the above medium for 4–5 days at 37°C before cytochemical experiments. HUVECs (human umbilical vein endothelial cells) were grown in Vascular medium from LifeLine (Cell Technology) for 5 days at 37°C humidified atmosphere and 5% CO_2. Some cultures were incubated with nicotine at different concentrations and for different lengths of time. The cells were expanded and used at no later than passage 12.

ACUTE CHOLESTEROL DEPLETION

Cells were treated with CDx in PBS for various periods at 37°C to acutely deplete their cholesterol content prior to fluorescent labeling as previously described [Borroni et al., 2007].

WIDE-FIELD FLUORESCENCE MICROSCOPY

Cells were stained for 1 h at 4°C with Alexa[488]α-bungarotoxin (Alexa[488]αBTX, 1 µg/mL) or with 0.5 µM fPEG-Chol for 10 min at 4°C, with or without 50 µM nicotine, washed and observed live or fixed with 4% paraformaldehyde for 15 min at 4°C followed by an additional 15 min fixation at room temperature. Alternatively, immunostaining of cells was carried out using anti-α7AChR rabbit polyclonal antibody (1:300 dilution) for 1 h, and anti-rabbit secondary antibody conjugated with Alexa[546] or Alexa[488] (1:400 dilution) for 1 h on ice. Excess label was removed by washing with PBS prior to microscopy. Cells were examined with a Nikon Eclipse E-600 microscope. Imaging was accomplished with a SBIG model ST-7 digital charge-coupled device camera (765 × 510 pixels, 9.0 × 9.0 µm pixel size; Santa Barbara, CA). The ST-7 CCD camera was driven by the CCDOPS software package (SBIG Astronomical Instruments, version 5.02). In all experiments, 40× (1.0 N.A.) or 60× (1.4 N.A.) Nikon planapochromatic oil-immersion objectives were used. Appropriate dichroic and emission filters were employed to avoid crossover of fluorescence emission. Eight-bit or 16-bit TIFF images were exported for further off-line analysis.

QUANTITATIVE IMAGE ANALYSIS

Fluorescence intensities of the 8- or 16-bit image were analyzed after manually outlining regions of interest (ROI) with the software Image J (NIH, Bethesda, MD). The average fluorescence intensity of a given ROI was measured within the αBTX-positive region of the cell and the average fluorescence intensity of an area of the same size positioned over an αBTX-negative region outside the cell was subtracted. These measurements were undertaken on randomly chosen cells, selected from phase-contrast images to avoid bias, for each experimental condition. For illustration purposes, images were processed using Adobe Photoshop, scaled with identical parameters, and pseudo-colored according to a custom designed look-up-table (LUT).

LABELING AND ISOLATION OF THE PLASMA MEMBRANE AND SOLUBLE AND INSOLUBLE FRACTIONS IN DETERGENT

Cells (70–80% confluent) were incubated with 0.1–100 nM [^{125}I]αBTX (specific activity 20 mCi/µmol) in the culture medium at room temperature for 3 h. They were subsequently scraped and resuspended in homogenization buffer (HB) prepared with 10 mM Tris, pH 7.4, containing 0.25 M sucrose, 1 mM EDTA, and protease inhibitors (1 mM PMSF, 1 mM pepstatin, 1 mM Leupeptin, 0.5 mg/mL Aprotinin, and 1 mM benzamidin). The homogenate was centrifuged at 8,500g for 10 min at 4°C. The pellet was discarded and the supernatants were centrifuged in a TXL 100 rotor at 40,000g for 30 min at 4°C in a Beckman Optima TXL centrifuge. Plasma membranes were lysed at 4°C for 20 min with Triton X-100 (TX-100) at 1% (v/v) in TNE (25 mM Tris-HCl, pH 7.5, containing 150 mM NaCl and 5 mM EDTA). They were subsequently centrifuged at 120,000g for 45 min at 4°C. For the sucrose gradient experiments, cells were divided into two groups and were labeled as above. The cell monolayers were rinsed with phosphate-buffered saline (150 mM NaCl, 20 mM sodium phosphate, pH 7.4) and lysed for 20 min in 0.5–1 mL of TNE/Triton X-100 (TX-100) buffer (25 mM Tris-HCl, pH 7.5, containing 150 mM NaCl, 5 mM EDTA, and 1% Triton X-100). The lysates were scraped from the dish with a rubber policeman, homogenized with 10 strokes in a Dounce homogenizer, and the dishes were rinsed with TNE/TX-100. The lysates were brought to 40% sucrose using 80% sucrose in TNT without TX-100 and placed in ultracentrifuge tubes. A linear sucrose gradient (5–30% in TNE without TX-100) was layered over the lysate. Gradients were centrifuged for 15–22 h at 39,000 rpm (200.000g) at 4°C in a Beckman SW41 rotor. Fractions (1 mL each) were collected from the top [Brown and Rose, 1992]. Aliquots were taken to measure radioactivity and protein content. Other aliquots were kept at −20°C to further analyze their components by Western blotting.

WESTERN BLOT ANALYSIS

The protein composition of the subcellular fractions was analyzed by SDS 10% polyacrylamide gel electrophoresis. Proteins were transferred to a polyvinylidene difluoride (PVDF) membrane (Immobilon-P, Millipore, Bedford, MA) using a Mini Trans-Blot electrophoretic transfer cell (Bio-Rad Life Science Group, Hercules, CA) for 1 h. The blot was stained with 0.5% Ponceau S in 1% acetic acid to visualize proteins or subjected to immunoblotting. Membranes were blocked overnight at 4°C with T-TBS buffer

(20 mM Tris-HCl pH 7.5, containing 150 mM NaCl and 0.05% Tween-20) supplemented with 0.5% bovine serum albumin and 5% non-fat dry milk. Immunoblotting detection of α7AChR protein was performed overnight at room temperature using a 4:5,000 dilution of H-302 rabbit anti-human α7AChR followed by incubation for 2 h at room temperature in a 1:10,000 dilution of goat anti-rabbit antibody conjugated to horseradish peroxidase. Immunoreactive bands were detected using the enhanced chemiluminescence Plus Western blotting kit (GE Healthcare UK Limited, UK).

[^{125}I]αBTX BINDING EXPERIMENTS

Iodination of αBTX was carried out using 250 μM ^{125}INa in 100 mM phosphate buffer. The resulting specific activity was 20 mCi/μmol. Surface AChR expression was determined by incubating confluent cells with increasing concentrations (0.1–100 nM) of [^{125}I]αBTX in cell culture medium for 4 h at 4°C. At the end of the incubation period, dishes were washed twice with Dulbecco's phosphate-buffered saline, cells were removed by scraping, and collected with 0.1 N NaOH. Radioactivity was measured in a γ counter with an efficiency of 80%. Non-specific binding was determined from the radioactivity remaining in the dishes after initial pre-incubation of the cells in 1 mM nicotine before addition of [^{125}I]αBTX. Non-specific binding amounted to 10% in control and treated cells. In order to determine the affinity of the radioactive toxin for the α7AChR expressed by endothelial cells, assays were carried out in culture plates as a function of time. Controls were carried out using cold αBTX and the full agonist carbamoylcholine. For other binding assays, cells were pre-incubated with 50–100 μM nicotine for 48 h, rinsed and incubated with [^{125}I]αBTX for 3 h at 37°C. Controls were made in the presence of excess nicotine.

FLUORESCENCE MEASUREMENTS

All fluorimetric measurements were performed in an SLM model 4800 fluorimeter (SLM Instruments, Urbana, IL) using a vertically polarized light beam from Hannovia 200-W mercury/xenon arc obtained with a Glan-Thompson polarizer (4-nm excitation and emission slits) and 0.7 mL quartz cuvettes. The temperature was set at 25°C with a thermostated circulating water bath (Haake, Darmstadt, Germany).

GENERALIZED POLARIZATION (GP) MEASUREMENTS

Plasma membrane fractions isolated from control HUVECs, or cells pre-incubated with 50 μM nicotine for 48 h were rinsed, labeled with Laurdan to give a final probe concentration of 0.6 μM and incubated in the dark for 40 min. GP values were calculated from Laurdan spectra obtained under direct excitation or FRET conditions, respectively, as in Antollini et al. [1996]. For the crystal violet (CrV) fluorescent measurements, the probe was dissolved in 10 mM buffer phosphate at three different stock concentrations (10, 50, and 350 μM) and stored at -20°C prior to titration experiments. Plasma membrane fractions from control and 50 μM nicotine-treated HUVEC during 48 h were suspended in 10 mM phosphate buffer. Two different conditions were studied: α7AChR in the resting state and α7AChR in the desensitized state (obtained by addition of 250 μM nicotine before CrV titration).The samples were titrated with increasing concentrations of CrV. After each addition, the samples were incubated for 15 min to allow for equilibration, and the emission spectra were collected from 605 to 700 nm using 600 nm excitation. A background spectrum (obtained from the same cuvette before CrV addition) was subtracted from the emission spectra obtained in the presence of CrV, and the maximum intensity (at 623–625 nm) was measured. To determine the CrV dissociation constant (K_D), the value of CrV maximum fluorescence emission was plotted as a function of the logarithmic CrV concentration (in moles). The resulting sigmoid curve was fitted to the Boltzmann function, and the K_D was calculated.

CELL MIGRATION ASSAY UNDER CONTROL AND CHOLESTEROL–DEPLETION CONDITIONS

Endothelial cells were grown to confluence in vascular medium as described above. The injury was made with a sterile tip under aseptic conditions on glass coverslips, in the presence or absence of 50 μM nicotine, with or without prior treatment with CDx (4 mM for 45 min).

PHARMACOLOGICAL DATA ANALYSIS

Crude data obtained from saturation isotherms, as well as the transformed Scatchard plots, association kinetic constants, ligand-displacement experiments, and half-life of the cell-surface α7AChR were analyzed using the software Origin 6.0. Statistical parameters were determined by the Student's t-test (two-tailed).

OTHER ANALYTICAL METHODS

Proteins were determined using the DC Protein Assay (Bio-Rad Life Science Group, Hercules, S.A.) or the method of Lowry et al. [1951].

INTRODUCTION

Nicotinic acetylcholine receptors (AChR) are integral membrane proteins that belong to the superfamily of Cys-loop receptors within the super-superfamily of ligand-gated ion channels (LGIC). They are pentameric complexes generated through various combinations of subunits that give rise to diverse forms of AChRs in the central (CNS) and peripheral (PNS) nervous systems, their function varying accordingly [Barrantes, 2004]. The α7-type acetylcholine receptor (α7AChR) is one of the most abundant subtypes in the CNS, and also occurs in non-nervous tissues such as vascular endothelium, bronchial tissue, macrophages and others. Neuronal AChRs that are homo-oligomers of α7 subunits have unusual properties making them especially interesting candidates for mediating "hormonal" functions of acetylcholine (ACh) in non-neural tissues, and perhaps also in excitable cells when expressed at extrasynaptic locations. Firstly, α7AChRs are activated not only by ACh but also by its natural metabolite, choline [Papke et al., 1996; Alkondon et al., 1997], upon cleavage of the endogenous ligand by acetylcholinesterase. Secondly, α7AChRs exhibit an unusually high permeability to Ca^{2+} [Seguela et al., 1993; Albuquerque et al., 1995] and changes in intracellular Ca^{2+} may result in a variety of metabolic effects.

Thus, α7AChRs exhibit both ionotropic and metabotropic-like properties.

α7AChRs perform various other functions in non-neuronal, non-excitable cells, and are considered key players in angiogenesis: α7AChRs modulate blood vessel formation and remodeling, and mediate the effect of nicotine (or the endogenous active neurotransmitter ACh) on angiogenesis [Heeschen et al., 2002]. Endothelial cell migration is an essential component of angiogenesis and endothelial regeneration after blood vessel injury. In an *in vitro* angiogenesis model, the antagonist mecamylamine was shown to completely and reversibly inhibit endothelial network formation [Heeschen et al., 2002]. The selective α7AChR antagonist, α-bungarotoxin, also inhibited endothelial tube formation.

In the CNS α7AChRs are involved in various disease conditions ranging from schizophrenia, epilepsy and Alzheimer's disease, to myasthenia gravis, congenital myasthenic syndromes, and inflammation in the case of the PNS [Cooke, 2007]. Angiogenesis and inflammation are co-dependent processes: inflammatory mediators promote angiogenesis directly and/or indirectly, and angiogenesis contributes to inflammatory pathology [Jackson et al., 1997]. Nicotine acts on endothelial AChRs activating endothelial cells and thus contributing to pathological angiogenesis. It has recently been found that α9 and α7AChRs have opposite effects on nicotine-induced cell proliferation and survival [Wu et al., 2009]. Membrane cholesterol accumulation is one of the first elements in the cascade leading to atherosclerotic plate growth. Heeschen and co-workers [Heeschen et al., 2006] demonstrated that the nicotine stimulation of hypercholesterolemic mice (a mutant deficient in ApoE lipoprotein) provokes the growth of atherosclerotic plates by increasing vasculature injury, angiogenesis and thrombosis. With this background in mind, the present work was conducted with the aim of investigating whether α7AChR cell-surface expression under nicotine stimulation (the "up-regulation" phenomenon) affects the cellular distribution, affinity state and conformation, occurrence in cholesterol-enriched ("raft"-like) subcellular fractions and other properties, with the ultimate aim of identifying possible relationships between nicotine-induced inflammatory stress and cholesterol levels in endothelial cells. Characterizing the participation of the α7AChR in endothelial pathology, as conceived in the present work, is key to understanding the molecular and cellular basis of tobacco-related diseases such as malignancy, atherosclerosis, and age-related macular degeneration.

IDENTIFICATION OF THE ENDOTHELIAL PROGENY

To confirm the identity of the endothelial cells, both HUVEC and RAEC cells were labeled with anti-CD34 antibody. Alexa[546]-conjugated secondary antibody in conjunction with primary antibody against the glycoprotein CD34 revealed discrete spots at the plasma membrane of HUVECs and RAECs (Supplementary Material Fig. 1). CD34 is one of the endothelial progenitor cell markers that is down-regulated in differentiated endothelial cells [Sandstedt et al., 2010], and hence the higher fluorescence intensity in HUVEC in comparison to the RAECs can be attributed to higher levels of expression and/or higher degree of differentiation of the HUVECs.

NICOTINE–INDUCED UP–REGULATION OF α7AChR IN VASCULAR ENDOTHELIAL CELLS

The α7AChR in vascular endothelial cells has been reported to be up-regulated by chronic nicotine treatment [Li and Wang, 2006]. In an initial series of experiments, we investigated the effect of different concentrations of nicotine on AChR cell-surface levels in the HUVEC line. The survival of cells did not appear to be affected by low concentrations (1 μM) of nicotine for several days. As shown in Figure 1A, the HUVEC cells survived for periods as long as 7 days showing neither morphological changes nor variations in the levels of AChR expression with respect to control cells. That is, the extremely low endogenous expression of α7AChR in HUVECs does not appear to be boosted by persistent application of low concentrations of nicotine to the cell culture. Endogenous α7AChR levels are very low (see below) and the fluorescence of the specific ligand Alexa[488]αBTX was barely visible under conventional wide-field fluorescence microscopy.

Subsequent studies with higher nicotine concentrations for shorter periods are shown in Figure 1B–D. As shown in Figure 1B, upon incubation with 50 μM nicotine for 24 h there were no changes in the cell-surface levels of AChR. However, α7AChR expression increased upon increasing exposure to the agonist to 48 h (Fig. 1C), as revealed by the fluorescence of Alexa[488]αBTX. At 72 h (Fig. 1D) the changes in expression levels were similar to those observed at 48 h, but under these conditions about 40% of the endothelial cells exhibited some degree of deleterious changes in their overall morphology and the number of dead cells increased significantly.

The changes in fluorescence intensity between control cells and those treated with different concentrations of nicotine for different periods are shown in Figure 1E. When the low fluorescence intensity of the control cells was normalized to 100%, it is clear that the chronic 7-day treatment of the cell cultures with 1 μM nicotine did not produce statistically significant changes in AChR expression levels. In contrast, treatment with 50 μM nicotine for shorter periods resulted in values about 300% higher than those of the control samples, which saturated at 48 h, without further increase at 72 h. Quantitative data of cells incubated for 48 h with 100 μM nicotine are also shown in the last column of Figure 1E. The fluorescence intensity increased with respect to control values, but cell viability was affected (Fig. 1F). Thus, the optimal nicotine-induced increase as judged by fluorescence labeling of the AChR was observed for nicotine concentrations of 50 μM and a time window of 48–72 h incubation. In order to verify the changes in fluorescent Alexa[488]αBTX brought about by nicotine exposure of the endothelial cells, an independent series of experiments was carried out using the radioactive derivative of the competitive antagonist ([125I]αBTX) and radioligand binding techniques. As shown in Figure 1G, cell-surface α7AChR increased from 53.3 ± 16 fmol/mg protein to 385.2 ± 46.8 fmol/mg protein upon exposure of cells to 50 μM nicotine.
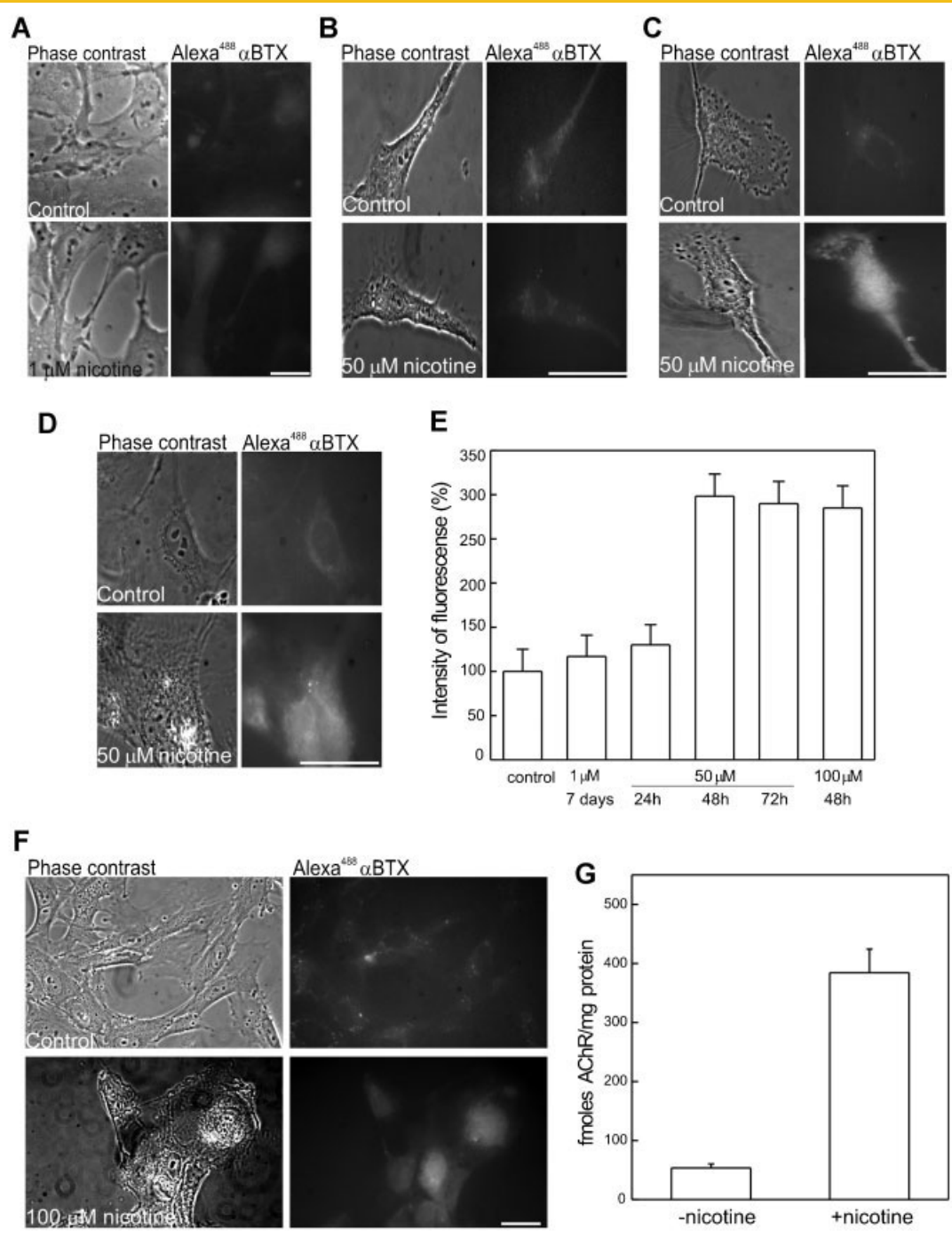
Fig. 1. Nicotine up–regulates α7AChR expression in human umbilical cord endothelial cells (HUVEC) in a time– and concentration–dependent manner: (A) HUVEC cells imaged in phase contrast (left column), and in epifluorescence mode (green channel, right column) to visualize cell–surface Alexa[488]αBTX. Control HUVEC cells (upper row) and cells incubated with 1 μM nicotine for 7 days (lower row). For the shorter agonist exposure, HUVECs were incubated with a higher (50 μM) level of nicotine for 24 h (B), 48 h (C), and 72 h (D), respectively, and stained with Alexa[488]αBTX. The images in the upper row correspond to control endothelial cells and in the lower row, cells incubated with nicotine. E: Relative fluorescence intensity measured in control and nicotine–treated cells as in Fig. 1 A, D, and F; $P < 0.05$ versus control. F: Phase contrast and fluorescence micrographs from control HUVEC cells (upper row) and cells treated with 100 μM nicotine for 48 h (lower row). Scale bar: 24 μm. G: Changes in [125I]αBTX binding upon treating cells with 100 μM nicotine for 48 h.
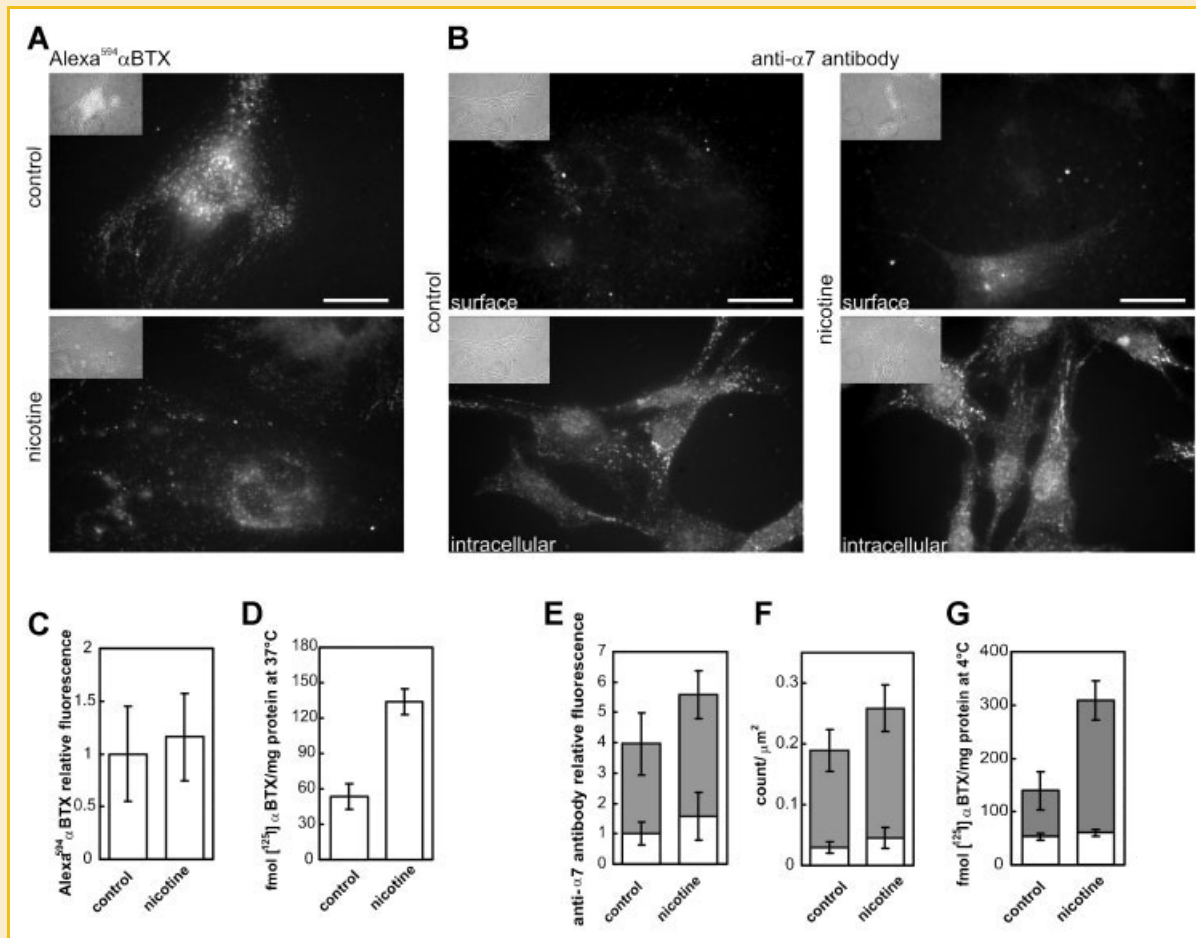
Fig. 2. Nicotine up-regulation of α7AChR in rat endothelial cells (RAECs) evidenced by fluorescence microscopy and radioactive α–bungarotoxin binding experiments: (A) Micrographs of cells stained with Alexa^{488}αBTX at 37°C for 4 h. Inset: Phase contrast. C: No statistically significant differences in relative fluorescence intensity are observed between control RAECs and cells treated with nicotine as in (A). D: [^{125}I]αBTX sites at 37°C in control and nicotine (50 μM for 48 h)–treated RAEC. B: Intracellular and cell-surface α7AChRs in RAECs were identified using anti–α7AChR goat polyclonal antibody followed by rabbit anti–goat Alexa^{488}-conjugated secondary antibody. Inset: Phase contrast. E: Quantitative data corresponding to wide–field fluorescence experiments as in (B), i.e., anti–α7 Alexa^{488}-conjugated secondary antibody relative fluorescence. F: Number of AChR clusters, expressed as counts per unit area (μm²) in surface and intracellular regions. G: Surface and intracellular [^{125}I]αBTX binding to RAECs at 4°C. Scale bar: 24 μm.

The endogenous α7AChR expression was assayed more in-depth in aortic endothelial cells, using a combination of radioligand binding experiments with [^{125}I]αBTX and wide-field fluorescence microscopy. Binding studies were performed at 37 and 4°C, with and without nicotine pre-incubation. The binding capacity of the RAECs (calculated mean B_{max}, 61.4 ± 3.9 fmol [^{125}I]αBTX/mg protein) was similar to that of HUVECs, with an affinity (K_D) of binding of 0.76 ± 0.1 nM (Supplementary Fig. 2). Given the very low expression at the cell surface, changes in surface receptor upon incubation with 50 μM nicotine for 48 h at 37°C were not apparent in fluorescence microscopy experiments after cell-surface AChR labeling with Alexa^{488}αBTX (Fig. 2A and C). As shown in Figure 2D, statistically significant differences were observed in radioiodinated toxin binding because of the higher sensitivity of the latter technique. Since at 37°C the apparent augmentation could be due to recycling of the receptor to the cell surface, a second series of experiments was performed at 4°C on both intact and permeabilized cells

(Fig. 2B). Cell-surface delivery and recycling are abolished at low temperatures, yet a 10-fold nicotine-induced increase in AChR levels was observed in the intracellular AChR pool.

Cell-surface and intracellular receptor levels were measured by immunofluorescence microscopy using specific rabbit anti-α7 primary antibodies followed by staining with anti-rabbit secondary antibody conjugated with Alexa^{488}. AChR at the plasmalemma was tagged with this combination in intact cells. To access intracellular receptor, cells were fixed with paraformaldehyde and permeabilized. As shown in Figure 2B, non-permeabilized, control RAECs were weakly stained with Alexa^{488}-conjugated goat anti-rabbit antibody. In contrast, permeabilized RAECs exhibited heavy staining, indicating a major proportion of α7AChR protein in intracellular compartments (Fig. 2B and E–G). Upon incubation with nicotine, a clear increase in α7AChR levels was apparent, both at the cell-surface and in intracellular compartments (Fig. 2B and E–G).
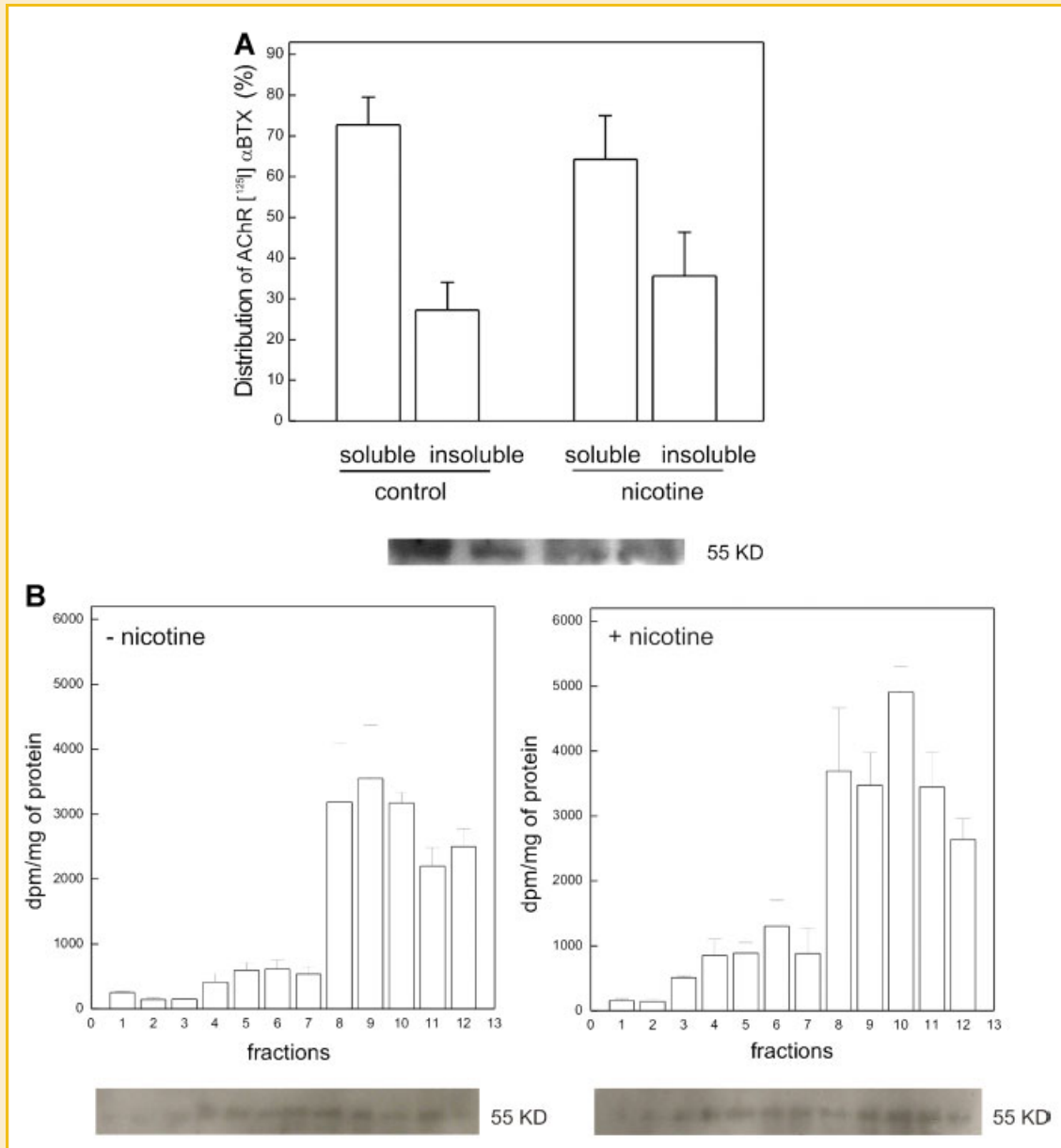
Fig. 3. Nicotine up–regulation of α7AChR in detergent extracts from HUVEC plasma membranes: (A) Percentage distribution of αBTX radioactivity in crude detergent–soluble and –insoluble fractions of plasma membranes from HUVEC cells incubated with 20–50 nM [^{125}I]αBTX (n = 4). Upon incubation with the toxin, cells were lysed for 20 min at 4°C in TNE buffer containing 1% Triton X–100, ultracentrifuged, and counted for radioactivity as detailed under Methods section. A Western blot showing the distribution of α7AChR between soluble and insoluble detergent samples (25 μg protein/lane) was performed using a 4:5,000 dilution of rabbit H–302 anti–α7 AChR polyclonal antibody. This immunoblot is a representative sample of four independent experiments. B: Radioactivity distribution in the sucrose gradient fractions obtained from lysates of control (left graph) and HUVEC cells treated with 50 μM nicotine for 48 h (right graph). Cells were incubated with [^{125}I]αBTX and lysed with TNE containing 1% Triton X–100. The lysates were brought to 40% sucrose using 80% stock sucrose solution and placed in ultracentrifuge tubes. A linear sucrose gradient was layered over the lysates. Fractions (1 mL each) were collected from the top. Immunoblot detection (10 μg protein/lane) of α7AChR was performed using 4:5,000 dilution of rabbit H–302 anti–α7 AChR polyclonal antibody. Images were analyzed using NIH ImageJ.

THE MAJORITY OF THE CELL-SURFACE α7AChR IN ENDOTHELIAL CELLS IS ASSOCIATED WITH DETERGENT-SOLUBLE MEMBRANES

Subcellular fractionation techniques in combination with cold 1% TX-100 extraction were applied next to isolate plasma membrane-enriched fractions from HUVECs. These two techniques yield not only plasmalemma-enriched fractions but resolve these into detergent-soluble and insoluble fractions (also termed detergent-resistant, DRM, and detergent-soluble, DSM membrane fractions, respectively), the biochemical operational definition of lipid "rafts" [Brown and Rose, 1992]. Figure 3A shows the distribution of [^{125}I]αBTX radioactivity in detergent-soluble and -insoluble fractions of plasma membranes prepared from control HUVECs

and from cells treated with 50 µM nicotine for 48 h. The majority of the AChR-[^{125}I]αBTX complex occurs in the DSM fraction (∼70%). Interestingly, the proportion of α7AChR in the DRM increased ∼10% in nicotine-treated samples (Fig. 3A).

In another series of experiments, HUVEC cells were subjected to subcellular fractionation and the distribution of the α7AChR was studied using a gradient centrifugation assay. As shown in Figure 3B, the distribution of radioactivity in gradient fractions from control HUVECs did not differ from that in cells treated with 50 µM nicotine for 48 h. In both cases the radioactive label was mainly found in the so-called heavy fractions, indicating the absence of redistribution of the α7AChR upon nicotine stimulation. This profile is comparable to that observed with endogenous expression levels of α7AChR in neuroepithelial cell lines like the SHSY5Y cells as reported by Cooper and Millar [1997].

CHANGES IN CHOLESTEROL CONTENT AFFECT THE α7AChR CELL–SURFACE CONTENT

In order to determine whether changes in endogenous cholesterol levels modify cell-surface AChR expression levels, HUVECs and RAECs were treated with different concentrations of CDx to cause cholesterol depletion [Borroni et al., 2007]. The degree of modification of the cholesterol content produced by CDx treatment was measured by labeling with the fluorescent cholesterol probe, fPEG-Chol. In parallel, the same property was measured using a colorimetric cholesterol oxidase assay. After fixing, cells were stained with fPEG-Chol for 10 min at RT. Lower concentrations of CDx than those used in previous studies [Borroni et al., 2007] were found to be sufficient to accomplish 50% cholesterol depletion in endothelial cells. Concentrations of ∼4–8 mM CDx were optimal for HUVEC (Fig. 4B and D). Concentrations higher than 8 mM CDx had a deleterious effect on morphology and cell viability in HUVECs. RAECs appeared to be more sturdy with regard to CDx-mediated cholesterol depletion: At the highest concentrations tested (16 mM CDx), no changes in cell morphology were observed within 45 min. Cholesterol content decreased in a concentration-dependent manner up to ∼75% with 16 mM CDx in RAEC (Fig. 4E); 4 mM CDx treatment attained ∼45% diminution.

Several studies have shown that CDx is capable of removing cholesterol from both low- and high-density membrane fractions, suggesting that cholesterol is removed from both "raft" and "non-raft" compartments [Zidovetzki and Levitan, 2007]. [^{125}I]αBTX binding assays on detergent-soluble and -insoluble fractions from HUVEC plasma membranes showed that the amount of this competitive antagonist bound to the cell surface diminished upon treatment with 4 mM CDx for 45 min at 37°C (∼50% decrease, Fig. 4F), affecting both plasma membrane fractions.

PHYSYCAL STATE OF THE ENDOTHELIAL PLASMALEMMA

To learn about the physical state of the plasma membrane in which the α7AChR is inserted in the endothelial cell, and of the lipid belt region surrounding the receptor protein in particular, we resorted to the amphiphilic fluorescent probe Laurdan (6-dodecanoyl-2-dimethylaminonaphthalene). This probe is a faithful reporter of the degree of water penetration and has been successfully employed in vitro and in intact cells [Barrantes, 2004; Fernandez Nievas et al., 2008]. Direct excitation of the probe senses the overall membrane "polarity," whereas excitation under Förster energy transfer conditions (FRET) provides information on the protein-vicinal lipid belt region [Antollini and Barrantes, 1998]. GP values of plasma membrane from control and nicotine-treated HUVEC were similar for conditions of direct excitation (control, 0.470; nicotine-treated cells, 0.478) and FRET (control, 0.502 and nicotine treated samples, 0.479, n = 2).

THE AFFINITY OF THE CELL–SURFACE α7AChR INCREASES UPON NICOTINE TREATMENT

To learn about the AChR conformational state, we employed crystal violet (CrV), an open channel blocker with fluorescence properties [Lurtz and Pedersen, 1999]. This probe exhibits a higher affinity for the desensitized state than for the resting state of the *Torpedo* muscle-type AChR [Fernandez Nievas et al., 2008] and, to our knowledge, has not been used so far on α7AChR. Here we found that the α7AChR in endothelial cells exhibited sub-micromolar affinities for CrV and underwent agonist-induced conformational changes. Thus, the K_D for the resting state 363.4 nM (n = 2) was reduced almost twofold to 177 nM (n = 2) upon treating the receptor-rich membranes with a desensitizing concentration of nicotine (Fig. 5).

NICOTINE AND CHOLESTEROL AFFECT ENDOTHELIAL CELL MIGRATION

Given the key importance of cell migration in angiogenesis, experiments were undertaken to evaluate the migration capacity of HUVECs in vitro. The assay consists of making a standard wound on the cell culture with a tip under aseptic conditions and following the ability of the cells to recover from this mechanical injury and migrate to fill up the empty surface [van Amerongen et al., 2007]. Figure 6A shows the temporal evolution of the wound repair in a time window of 48 h and the effect of nicotine on this phenomenon. Treatment with 50 µM nicotine significantly stimulated cell growth with respect to control levels; the wound was almost fully recovered after 48 h (Fig. 6A). Figure 6B shows that nicotine induces statistically significant changes in the wound recovery ability of HUVECs, accelerating the repair mechanism. Furthermore, although cholesterol depletion mediated by CDx treatment had little if any effect per se on cell migration (Fig. 6A), the positive effect of nicotine on wound repair drastically diminished in cells deprived of the sterol.

DISCUSSION

Radioligand binding studies enabled the determination of the endogenous levels of α7AChR expression in both venous and aortic endothelial cells (HUVEC and RAEC, respectively) at very low levels (B_{max} was 53 ± 6.6 fmol/mg of protein in HUVEC and
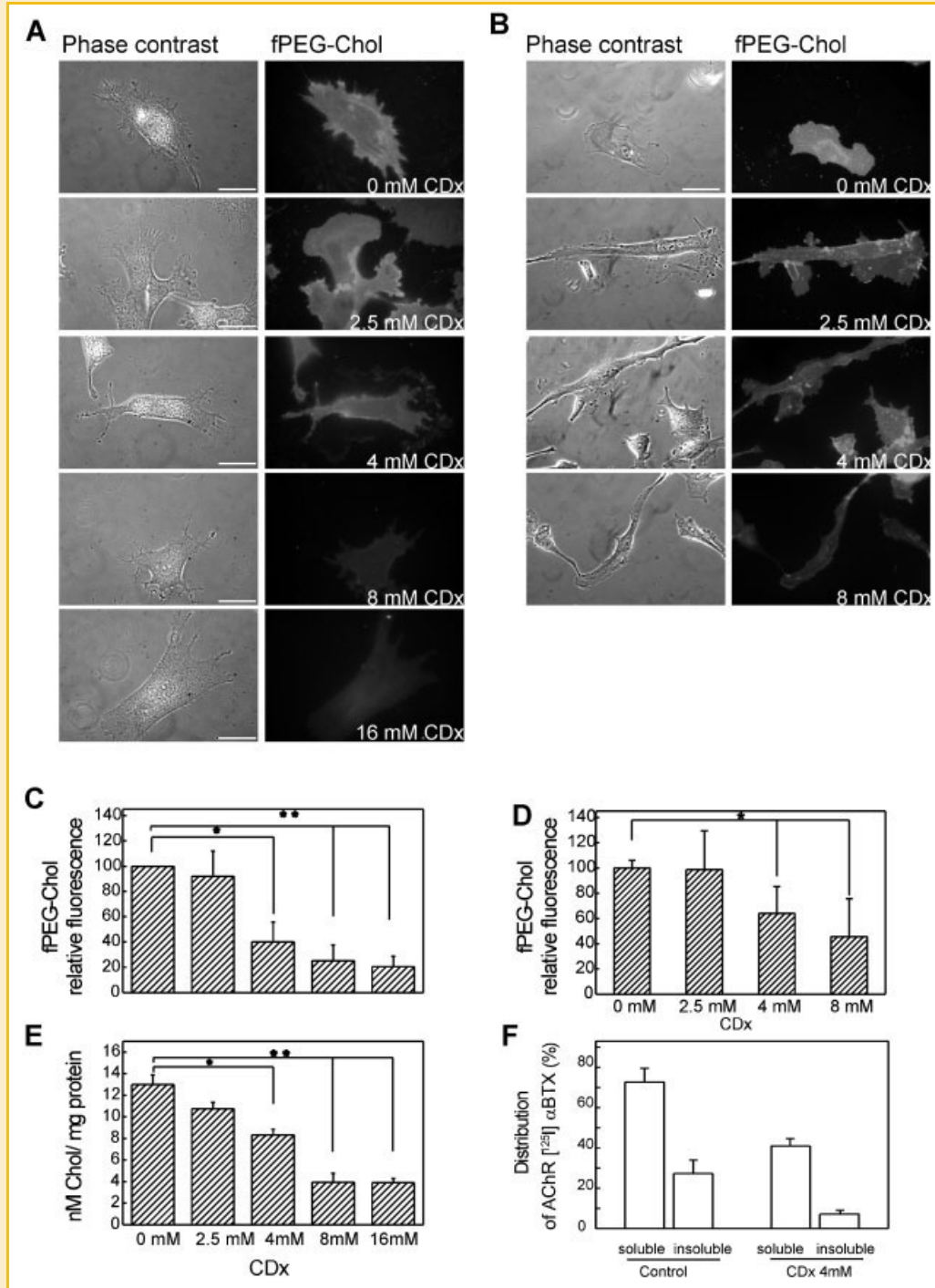
Fig. 4. Effects of cholesterol depletion of endothelial cells on distribution of the fluorescent probe fPEG-Chol: (A) RAECs and (B) HUVECs treated with CDx for 45 min at the indicated concentrations (left column, phase contrast, and fPEG-Chol fluorescence, right column). Cells were labeled with the fluorescent cholesterol analog fPEG-Chol (0.5 μM) for 10 min before fixation with paraformaldehyde. Scale bar: 26 μm. C and D: Quantification of fPEG-Chol cell-surface fluorescence in RAECs and HUVECs, respectively. The asterisk indicates statistically significant differences between control and CDx-treated cells; $^*P < 0.02$ and $^{**}P < 0.01$ in (C); $^*P < 0.05$ versus control in (D). E: Quantification of cellular cholesterol from RAECs; data are expressed as nmole cholesterol/mg of protein and are the mean ± SD of three individual samples ($^*P < 0.05$ and $^{**}P < 0.02$ with respect to control values). F: Effect of cholesterol depletion or HUVECs on the distribution of AChR into detergent-soluble and detergent-resistant fractions. Cells were treated with 4 mM CDx for 40 min, washed thrice, incubated with 10 nM [^{125}I]αBTX for 2 h, and subjected to detergent extraction and subcellular fractionation as detailed under Methods section.
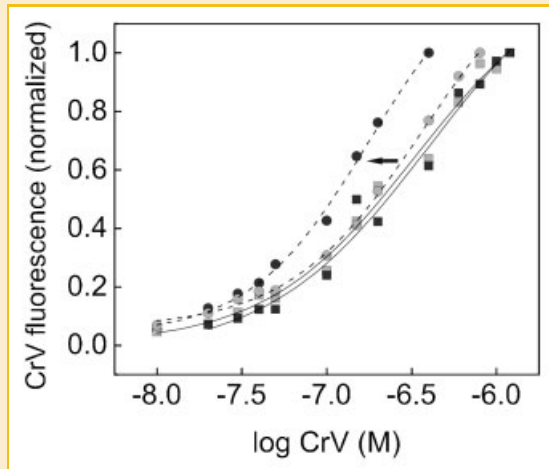
Fig. 5. Conformational state and apparent equilibrium dissociation constant, K_D, of the channel blocker CrV for the α7AChR: HUVECs were cultured for 48 h with (---) or without (—) addition of 50 μM nicotine. Plasma membrane fractions were prepared from the two batches of cells, and titrated with CrV in the absence ($\blacksquare$, $\bullet$) or presence ($\blacksquare$, $\bullet$) of an activating and desensitizing concentration of full agonist (250 μM nicotine). The K_D corresponding to the resting state ($\blacksquare$) = 333.8 nM, K_D ($\blacksquare$) = 402.7 nM, and to membranes treated with nicotine ($\bullet$) = 363.4 nM, K_D ($\bullet$) = 177 nM were obtained by fitting a Boltzmann equation to the experimental data points. Similar experiments carried out on cells which were not up-regulated by nicotine exposure in the culture medium were too noisy (because of the negligible amount of AChR, see text).

61.4 ± 3.9 fmol/mg of protein in RAEC). Treatment with nicotine in HUVECs was found to up-regulate these levels sevenfold with respect to controls (Fig. 1G). These levels of AChR expression are comparable to the endogenous expression levels of α7AChR in neuroepithelial cell lines like the SHSY5Y cells (50 fmol/mg protein [Peng et al., 1999] or 45 fmol/mg protein [Cooper and Millar, 1997]).

Conditions are described under which the agonist nicotine increases cell-surface α7AChRs having the ability to bind the competitive antagonist α-BTX. This increase is usually referred to as up-regulation and implies enhanced functional ability but not necessarily augmented amounts of total receptors. Nicotine plasma concentration in active and passive smokers ranges between 10^{-6} and 10^{-8} M [Benowitz et al., 1984], with a peak level occurring within 10 min from smoking initiation and declining with an average elimination half-life of about 2 h [Keller-Stanislawski and Caspary, 1992]. In our study, the nicotine concentrations used were higher than those measured in the plasma of heavy smokers and significantly increased the expression of α7AChRs. Optimal agonist concentrations to boost receptor functional expression and cell-surface delivery were found to be in the order of ~50 μM (within the 48–72 h period). Similar concentrations were used by Xu et al. [2007] for activation of pulmonary sensory neurons, by Wang et al. [2004] for activation of macrophages and HUVECs, and by Buttigieg et al. [2008], who claimed that adrenomedullary chromaffin cells lose their hypoxic sensitivity when grown in culture for more than a week in the presence of 50 μM nicotine. We observed that extremely high nicotine doses (100 μM) induce endothelial cell swelling, large
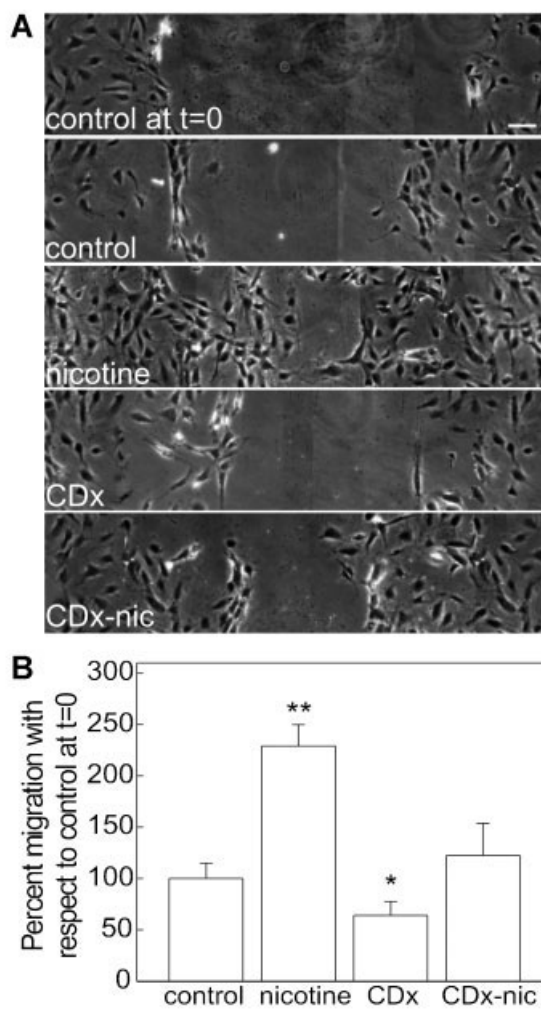

Fig. 6. Synergic effect of nicotine and cholesterol on wound–repair migration assay: (A) Collage of phase contrast images of HUVEC cells immediately after the mechanical injury (top image), which depleted cells from the central region of the coverslip. Subsequent micrographs correspond to representative examples of control cells 48 h after production of the wound (the wound has been ~40% repaired) and upon incubation with 50 μM nicotine for 48 h or with the same after Chol depletion with 4 mM CDx. B: Wound repair (%) in the experiments shown in (A). $^*P < 0.05$ and $^{**}P < 0.02$ versus control.

translucent cytoplasmatic inclusions and vacuolation, clear signs of cytotoxic effect. These concentrations, however, are much higher than those observed in human plasma of cigarette smokers [Benowitz et al., 1984]. The up-regulation of the α7AChR in vascular endothelium by high nicotine concentration treatment constitutes a phenomenon akin to that observed with the other most abundant AChR subtype in the central nervous system, namely the α4β2AChR [Corringer et al., 2006]. That is, the up-regulation phenomenon characteristically observed in the CNS-pathognomonic of nicotine addiction [Buisson and Bertrand, 2002] is also present in vascular endothelium. In brain, α4β2AChR stimulation by nicotine triggers a cascade starting with AChR activation and desensitization, followed by a long-term up-regulation phenome-

non manifested as an increase in the production of high-affinity AChRs, a paradoxical process that occurs in the brain of smokers. Here we show that the α7AChR in present in plasmalemma-enriched fractions from endothelial cells undergoes nicotine-induced transitions from a relatively low affinity (363.4 nM) to a higher affinity (177 nM) for the open-channel blocker CrV (Fig. 5). The diminution of the K_D values in nicotine-treated cells shows than α7AChR responds to nicotine by undergoing conformational changes towards high-affinity desensitized states, a characteristic which is most pronounced in α7AChRs [Dani and Bertrand, 2007]. The up-regulation phenomenon is initiated in the endoplasmic reticulum, soon after transduction of the receptor protein occurs [Sallette et al., 2005]. This has led to the suggestion [Lester et al., 2009] that nicotine exerts the role of a "maturational enhancer," eliciting up-regulation by promoting maturation of AChR precursors that would otherwise be degraded. Lester et al. [2009] hypothesized that nicotine plays the role of a "pharmacological chaperone" as a first step in a complex mechanism involving the chronic adaptation to the drug. In this context, addiction would be associated with an excess offer of the chaperone (nicotine).

In contrast to the agonist-induced up-regulation of the receptor, acute CDx-mediated cholesterol depletion resulted in a drastic diminution (≥50%) of the cell-surface AChR pool in endothelial cells (Fig. 4F), as was reported for CHO-K1/A5 cells [Borroni et al., 2007], suggesting a common operating mechanism: Acceleration of receptor endocytosis.

GP values of plasma membrane from control and nicotine-treated HUVEC were similar for conditions both of direct excitation and FRET, indicating that the endothelial cell membrane is highly ordered ("rigid") and that this physical characteristic is not modified by nicotine treatment. These physical properties of the plasmalemma are a reflection of the relatively high cholesterol content of the endothelial cell. In RAECs, cholesterol levels amounted to 13.1 ± 0.9 nmol cholesterol/mg protein (Fig. 4E, n = 3), and 15.9 nmol cholesterol/mg protein (n = 2) were found in HUVEC, similar to the values reported by [Kim et al., 1991] and 11 ± 2.5 nmol cholesterol/mg protein in CHO-K1/A5 cells [Pauly et al., 1998].

Nicotine is the major bioactive component of tobacco, and the pro-atherogenic mechanism of nicotine action is still largely speculative. It is clear, however, that nicotine acts on endothelial cells by activating AChRs and augmenting pathological angiogenesis [Wu et al., 2009]. Abnormal angiogenesis contributes to tobacco-related diseases such as cancer, atherosclerosis and age-related macular degeneration. Cell migration is a necessary step in angiogenesis, and experiments on the effect of the ligand on endothelial cell migration already provide some insights into nicotine action, showing that the drug favors the migration phenomenon. Our findings are consistent with previous observations that nicotine stimulates endothelial cell proliferation [Heeschen et al., 2002; Cooke, 2007]. In endothelial cells, α7AChR stimulation indirectly triggers activation of the integrin αvβ3 receptor and an intracellular MAP kinase (ERK) pathway that mediates angiogenesis [Arias et al., 2009]. Non-selective cholinergic agonists such as nicotine have been shown to induce angiogenesis, enhancing tumor progression [Arias et al., 2009].

Evidence is accumulating in support of Lindstrom's proposal that nicotine acts as a pharmacological chaperone for nascent AChR [Kuryatov et al., 2005]. Up-regulation by chronic nicotine induced in animal models and transfected cells is certainly not transcriptional and is probably post-translational, not requiring synaptic transmission or other diffusible extracellular signals [Pauly et al., 1998; Dani and Bertrand, 2007]. It is known that α7AChR needs less time than other AChRs to recover from desensitization after chronic nicotine treatment [Kawai and Berg, 2001]. The precise mechanism of AChR up-regulation is still unclear, and some authors suggest that long-term nicotine treatment could induce a structural modification and desensitization of AChRs [Fenster et al., 1997] resulting in a reduction in the turnover of AChRs recruited from the plasmalemma followed by an increase in cell-surface AChRs. Alternatively, maturation of AChRs due to increased efficacy of subunit assembly [Wang et al., 1998] or the isomerization of low affinity surface receptors into high-affinity receptors may also be involved in the increase at the cell surface [Buisson and Bertrand, 2002].

It is known that nicotine stimulation induces angiogenesis [Heeschen et al., 2002]. In this respect, findings from our study and others show that α7AChR in endothelial cells is up-regulated by this drug, causing cell migration and proliferation. Thus, α7AChR appears to behave as a key intermediate molecule in triggering nicotinic responses in endothelium, thus playing a pivotal role in improving endothelial cell survival and, ultimately, therapeutic efficacy. The extremely low endogenous expression of α7AChR in endothelial cells does not appear to be boosted by persistent application of low concentrations of nicotine. In our hands, the up-regulation of α7AChR occurs at high nicotine doses, at a concentration range proposed as therapeutic for different disease conditions [Kleinsasser et al., 2005; Hong et al., 2009]. These concentrations are at a threshold value beyond which cellular damage is produced. Harmful nicotine effects might also be induced by other smoke constituents in vivo. This seems not to be the case for nicotine replacement therapy and α7AChR could be a potential target for therapeutic modulation in disorders of pathological or insufficient angiogenesis.

ACKNOWLEDGMENTS

REFERENCES

Albuquerque EX, Pereira EF, Castro NG, Alkondon M, Reinhardt S, Schroder H, Maelicke A. 1995. Nicotinic receptor function in the mammalian central nervous system. Ann NY Acad Sci 757:48–72.

Alkondon M, Pereira EF, Cortes WS, Maelicke A, Albuquerque EX. 1997. Choline is a selective agonist of alpha7 nicotinic acetylcholine receptors in the rat brain neurons. Eur J Neurosci 9:2734–2742.

Antollini SS, Barrantes FJ. 1998. Disclosure of discrete sites for phospholipid and sterols at the protein-lipid interface in native acetylcholine receptor-rich membrane. Biochemistry 37:16653–16662.

Antollini SS, Soto MA, Bonini de Romanelli Gutiérrez I, Merino C, Sotomayor P, Barrantes FJ. 1996. Physical state of bulk and protein-associated lipid in nicotinic acetylcholine receptor-rich membrane studied by Laurdan generalized polarization and fluorescence energy transfer. Biophys J 70:1275–1284.

Arias HR, Richards VE, Ng D, Ghafoori ME, Le V, Mousa SA. 2009. Role of non-neuronal nicotinic acetylcholine receptors in angiogenesis. Int J Biochem Cell Biol 41:1441–1451.

Barrantes FJ. 2004. Structural basis for lipid modulation of nicotinic acetylcholine receptor function. Brain Res Brain Res Rev 47:71–95.

Benowitz L, Kuyt F, Jacob P. 1984. Influence of nicotine on cardiovascular and hormonal effects of cigarette smoking. Clin Pharmacol Ther 36:74–81.

Borroni V, Baier CJ, Lang T, Bonini I, White MM, Garbus I, Barrantes FJ. 2007. Cholesterol depletion activates rapid internalization of submicron-sized acetylcholine receptor domains at the cell membrane. Mol Membr Biol 24:1–15.

Brown DA, Rose JK. 1992. Sorting of GPI-anchored proteins to glycolipid-enriched membrane subdomains during transport to the apical cell surface. Cell 68:533–544.

Buisson B, Bertrand D. 2002. Nicotine addiction: The possible role of functional upregulation. Trends Pharmacol Sci 23:130–136.

Buttigieg J, Brown S, Zhang M, Lowe M, Holloway AC, Nurse CA. 2008. Chronic nicotine in utero selectively suppresses hypoxic sensitivity in neonatal rat adrenal chromaffin cells. Faseb J 22:1317–1326.

Cooke JP. 2007. Angiogenesis and the role of the endothelial nicotinic acetylcholine receptor. Life Sci 80:2347–2351.

Cooper ST, Millar NS. 1997. Host cell-specific folding and assembly of the neuronal nicotinic acetylcholine receptor alpha7 subunit. J Neurochem 68:2140–2151.

Corringer PJ, Sallette J, Changeux JP. 2006. Nicotine enhances intracellular nicotinic receptor maturation: A novel mechanism of neural plasticity? J Physiol Paris 99:162–171.

Cutini P, Sellés J, Massheimer V. 2009. Cross-talk between rapid and long term effects of progesterone on vascular tissue. J Steroid Biochem Mol Biol 115:36–43.

Dani JA, Bertrand D. 2007. Nicotinic acetylcholine receptors and nicotinic cholinergic mechanisms of the central nervous system. Annu Rev Pharmacol Toxicol 47:699–729.

Fenster CP, Rains MF, Noerager B, Quick MW, Lester RA. 1997. Influence of subunit composition on desensitization of neuronal acetylcholine receptors at low concentrations of nicotine. J Neurosci 17:5747–5759.

Fernandez Nievas GA, Barrantes FJ, Antollini SS. 2008. Modulation of nicotinic acetylcholine receptor conformational state by free fatty acids and steroids. J Biol Chem 283:21478–21486.

Heeschen C, Chang E, Aicher A, Cooke JP. 2006. Endothelial progenitor cells participate in nicotine-mediated angiogenesis. J Am Coll Cardiol 48:2553–2560.

Heeschen C, Weis M, Aicher A, Dimmeler S, Cooke JP. 2002. A novel angiogenic pathway mediated by non-neuronal nicotinic acetylcholine receptors. J Clin Invest 110:527–536.

Hong DP, Fink AL, Uversky VN. 2009. Smoking and Parkinson's disease: Does nicotine affect alpha-synuclein fibrillation? Biochim Biophys Acta 1794:282–290.

Jackson JR, Seed MP, Kircher CH, Willoughby DA, Winkler JD. 1997. The codependence of angiogenesis and chronic inflammation. Faseb J 11:457–465.

Kawai H, Berg DK. 2001. Nicotinic acetylcholine receptors containing alpha 7 subunits on rat cortical neurons do not undergo long-lasting inactivation even when up-regulated by chronic nicotine exposure. J Neurochem 78:1367–1378.

Keller-Stanislawski B, Caspary S. 1992. Pharmacokinetics of nicotine and cotinine after application of two different nicotine patches under steady state conditions. Arzneimittelforschung 42:1160–1162.

Kim JA, Maxwell K, Hajjar DP, Berliner JA. 1991. Beta-VLDL increases endothelial cell plasma membrane cholesterol. J Lipid Res 32:1125–1131.

Kleinsasser NH, Sassen AW, Semmler MP, Harréus UA, Licht AK, Richter E. 2005. The tobacco alkaloid nicotine demonstrates genotoxicity in human tonsillar tissue and lymphocytes. Toxicol Sci 86:309–317.

Kuryatov A, Luo J, Cooper J, Lindstrom J. 2005. Nicotine acts as a pharmacological chaperone to up-regulate human alpha4beta2 acetylcholine receptors. Mol Pharmacol 68:1839–1851.

Lester HA, Xiao C, Srinivasan R, Son CD, Miwa J, Pantoja R, Banghart MR, Dougherty DA, Goate AM, Wang JC. 2009. Nicotine is a selective pharmacological chaperone of acetylcholine receptor number and stoichiometry. Implications for drug discovery. AAPS J 11:167–177.

Li XW, Wang H. 2006. Non-neuronal nicotinic alpha 7 receptor, a new endothelial target for revascularization. Life Sci 78:1863–1870.

Lowry OH, Rosebrough NJ, Farr AL, Randall RJ. 1951. Protein measurement with the Folin phenol reagent. J Biol Chem 193:265–275.

Lurtz MM, Pedersen SE. 1999. Aminotriarylmethane dyes are high-affinity noncompetitive antagonists of the nicotinic acetylcholine receptor. Mol Pharmacol 55:159–167.

Papke RL, Bencherif M, Lippiello P. 1996. An evaluation of neuronal nicotinic acetylcholine receptor activation by quaternary nitrogen compounds indicates that choline is selective for the alpha 7 subtype. Neurosci Lett 213:201–204.

Pauly JL, Lee HJ, Hurley EL, Cummings KM, Lesses JD, Streck RJ. 1998. Glass fiber contamination of cigarette filters: An additional health risk to the smoker? Cancer Epidemiol Biomarkers Prev 7:967–979.

Peng JH, Lucero L, Fryer J, Herl J, Leonard SS, Lukas RJ. 1999. Inducible, heterologous expression of human a7-nicotinic acetylcholine receptors in a native nicotinic receptor-null human clonal line. Brain Res 825:172–179.

Sallette J, Pons S, villers-Thiery A, Soudant M, Prado de CL, Changeux JP, Corringer PJ. 2005. Nicotine upregulates its own receptors through enhanced intracellular maturation. Neuron 46:595–607.

Sandstedt J, Jonsson M, Lindahl A, Jeppsson A, Asp J. 2010. C-kit+. Basic Res Cardiol 105:545–556.

Sato SB, Ishi K, Makino A, Iwabuchi K, Yamaji-Hasegawa A, Senoh Y, Nagaoka I, Sakuraba I, Kobayashi T. 2004. Distribution and transport of cholesterol-rich membrane domains monitored by a membrane-impermeant fluorescent polyethylene glycol-derivatized cholesterol. J Biol Chem 279:23790–23796.

Seguela P, Wadiche J, neley-Miller K, Dani JA, Patrick JW. 1993. Molecular cloning, functional properties, and distribution of rat brain alpha 7: A nicotinic cation channel highly permeable to calcium. J Neurosci 13:596–604.

van Amerongen MJ, Harmsen MC, van RN, Petersen AH, van Luyn MJ. 2007. Macrophage depletion impairs wound healing and increases left ventricular remodeling after myocardial injury in mice. Am J Pathol 170:818–829.

Yeh YC, Hwang GY, Liu IP, Yang VC. 2002. Identification and expression of scavenger receptor SR-BI in endothelial cells and smooth muscle cells of rat aorta in vitro and in vivo. Atherosclerosis 161:95–103.

Wang H, Wang X, Zhang S, Lou C. 1998. Nicotinic acetylcholine receptor is involved in acetylcholine regulating stomatal movement. Sci China C Life Sci 41:650–656.

Wang Y, Wang L, Ai X, Zhao J, Hao X, Lu Y, Qiao Z. 2004. Nicotine could augment adhesion molecule expression in human endothelial cells through macrophages secreting TNF-alpha, IL-1beta. Int Immunopharmacol 4:1675–1686.

Wu JC, Chruscinski A, De JP V, Singh H, Pitsiouni M, Rabinovitch M, Utz PJ, Cooke JP. 2009. Cholinergic modulation of angiogenesis: Role of the 7 nicotinic acetylcholine receptor. J Cell Biochem 108:433–446.

Xu J, Yang W, Zhang G, Gu Q, Lee LY. 2007. Calcium transient evoked by nicotine in isolated rat vagal pulmonary sensory neurons. Am J Physiol Lung Cell Mol Physiol 292:L54–L61.

Zidovetzki R, Levitan I. 2007. Use of cyclodextrins to manipulate plasma membrane cholesterol content: Evidence, misconceptions and control strategies. Biochim Biophys Acta 1768:1311–1324.